Terahertz imaging system using high-Tc superconducting oscillation devices

M. Tsujimoto, H. Minami, K. Delfanazari, M. Sawamura, R. Nakayama et al.

Related Articles

Monolithic high-temperature superconducting heterodyne Josephson frequency down-converter
Appl. Phys. Lett. 100, 262604 (2012)

Etching suspended superconducting tunnel junctions from a multilayer
Appl. Phys. Lett. 100, 252602 (2012)

Ferromagnetic Josephson switching device with high characteristic voltage
Appl. Phys. Lett. 100, 222601 (2012)

1/f noise of Josephson-junction-embedded microwave resonators at single photon energies and millikelvin temperatures
Appl. Phys. Lett. 100, 142601 (2012)

The influence of standing waves on synchronization and self-heating of Josephson junctions in resonant systems
Low Temp. Phys. 38, 321 (2012)

Additional information on J. Appl. Phys.

Journal Homepage: http://jap.aip.org/

Journal Information: http://jap.aip.org/about/about_the_journal

Top downloads: http://jap.aip.org/features/most_downloaded

Information for Authors: http://jap.aip.org/authors

Terahertz imaging system using high-T_c superconducting oscillation devices

M. Tsujimoto, H. Minami, K. Delfanazari, M. Sawamura, R. Nakayama, T. Kitamura, T. Yamamoto,[a] T. Kashiwagi, T. Hattori, and K. Kadowaki[b]

Graduate School of Pure and Applied Sciences, University of Tsukuba, 1-1-1 Tennodai, Tsukuba, Ibaraki 305-8573, Japan; CREST, Japan Science and Technology Agency, Kawaguchi Center Building, 4-1-8 Honcho, Kawaguchi, Saitama 332-0012, Japan; and WPI-MANA, 1-1 Namiki, Tsukuba, Ibaraki 305-0044, Japan

Microwatt power oscillation devices at sub-terahertz frequency region between 0.3 and 1.0 terahertz (THz) were fabricated from high-T_c superconducting single crystalline $Bi_2Sr_2CaCu_2O_{8+\delta}$ and used as a source of the transmission terahertz imaging system. As test examples, terahertz images of coins and a razor blade placed inside the brownish paper envelopes with the spatial resolution of 1 mm are presented. The signal-to-noise ratio exceeds 130 in these images. Using a simple wedge-shaped interferometer and analysing the interference fringe pattern, the wavelength of the terahertz wave is calibrated within 0.1% accuracy. This interferometer also provides a simple method to measure the absorption coefficient of the liquid sample. Two test measurements for distilled water and ethanol are demonstrated and their absorption coefficients are obtained with 99.2% accuracy. This suggests that our terahertz imaging system can be applied to many practical applications, such as biological and biomedical imaging, environmental monitoring, microanalysis of impurities, structure and dynamical analyses of large molecules and ions in solution. © *2012 American Institute of Physics*. [http://dx.doi.org/10.1063/1.4729799]

I. INTRODUCTION

The terahertz (THz) electromagnetic (EM) wave with a frequency span of 0.1–10 THz (1 THz = 10^{12} Hz) is known to be the most unique area in all EM spectra, since it is simply unavailable due to lack of compact and convenient radiation sources.[1] In the recent years, much effort has been put in to overcome the above difficulty, in particular, in the field of semiconductors and laser technologies. Resonant tunneling diodes,[2] uni-traveling-carrier photodiodes,[3] and quantum cascade laser,[4] have been developed as useful THz sources. Recently, graphene and carbon nanotubes have also been reported to be as good candidates for the THz wave generator.[5,6]

Since THz waves have the properties of being able to pass through various objects, such as plastics, paper, ceramics, semiconductors, liquids, and proteins similar to the radio waves, they enable us to image various cm-by-cm wide substances,[7] where the spatial resolution is actually determined by the wavelength of the THz wave, typically ∼1 mm. Also, since the irradiation damage to these soft objects is known to be negligibly small in contrast to the X-ray, in fact there is much demand for the nondestructive and noninvasive imaging technique in the field of the material inspection, medical diagnostic, security check, and environmental monitoring. Moreover, measuring the absorption spectrum in the THz region, where various molecular vibration modes of organic and high-molecular compounds dominate the EM wave absorption, one can identify the chemical substances both qualitatively and quantitatively. To realize these applications, compact, solid-state, and reliable THz

source devices are strongly desired in spite of their technical difficulties.

In 2007, we have discovered a remarkable phenomenon that the high transition temperature (T_c) superconducting $Bi_2Sr_2CaCu_2O_{8+\delta}$ (Bi-2212) compound generates intense and coherent EM waves in a THz frequency region.[8] This compound is known as the intrinsic Josephson junction (IJJ) system,[9] where the insulating Bi_2O_2 plane is sandwiched by CuO_2 double planes responsible for superconductivity. Since the distance between CuO_2 planes is only 1.533 nm but the superconducting coupling is extremely small, this system is known to behave as a multi-stack of IJJs. The THz EM wave is then generated by injecting dc current into a mesa structure, which is nano-engineered either by a focused ion beam or ion etching technique, in a rectangular shape of 45–100 μm in width, 300–400 μm in length, and 1–2 μm in thickness.[8,10–12] According to previous studies, the radiation frequency, f, is known to obey two necessary conditions: One is the Josephson relation[13] given by $f = f_J = (2e/h)V/N$, where e is the elementary charge, h the Planck's constant, V the applied voltage, and N the number of the active IJJs, implying that applying 1 mV produces the 0.4836 THz ac current. Another is the cavity resonance condition: in the case of the rectangular mesa, it can be written as $f = c_0/2nw$, where c_0 is the speed of light in vacuum, n the refractive index of Bi-2212, and w the width of the mesa.

Previous studies also found that the present IJJ system can be used as a terahertz oscillation device which emits continuous and microwatt power THz waves at tunable frequencies between 0.3 and 1.0 THz with the spectral linewidth of ∼0.5 GHz[14] and can be operated in power modulation mode at 500 kHz.[15] These device characteristics enable us to accumulate the data for individual measurement point at high resolution in a few milliseconds or less. In

[a]Present address: Quantum Beam Science Directorate, Japan Atomic Energy Agency, 1233 Watanuki-cho, Takasaki, Gunma 370-1292, Japan.
[b]Electronic mail: kadowaki@ims.tsukuba.ac.jp.

addition, the solid-state IJJ device is extremely small in size and its output power is stable enough during operation. Therefore, in this study, we have attempted to demonstrate the THz imaging experiment by using the IJJ oscillation devices as THz sources in order to promote effective use of the present IJJ device for various practical applications.

II. EXPERIMENTAL

The IJJ THz oscillation devices were assembled in a He-flow cryostat with two off-axis parabolic mirrors, scan stage and fast hot-electron (HE) bolometer as seen in Fig. 1. Two off-axis parabolic mirrors with focal lengths of 152.4 mm and 220 mm both with diameters of 75 mm are set to focus the THz waves at the sample position. The image object is fixed on the 2D scan stage (SIGMA KOKI Co., SGAMH26-200) and scanned in X (horizontal) and Z (vertical) directions at the variable speed below 130 mm/s. The practical maximum speed should be 80 mm/s, which corresponds to a 5-ms time constant per data point when the measurement step is set to sub-millimeter equivalent to the wavelength. Although the IJJ oscillation device can be modulated much faster as mentioned above, in the present setup the maximum scan speed only depends on the minimum time constant of the lock-in amplifier (EG&G instruments Co., 7265). Nevertheless, the actual imaging has been performed at the speed of 32 mm/s in order to obtain sufficient data points. Before starting the THz imaging, the optical path presented in Fig. 1 is precisely adjusted by referring the visible light from a light-emitting diode (LED) attached to the source position. A high-speed InSb HE bolometer (QMC Instruments Ltd., QFI/2BI) placed right behind the scan stage is used for measuring the output intensity of the THz waves passing through the sample. The current-voltage (I–V) characteristics of the IJJ device and the bolometer output are simultaneously monitored by two oscilloscopes (OSCs). A left lower photo in Fig. 1 shows the top views of the actual imaging system.

The IJJ oscillation device used in this study is schematically presented in the left inset of Fig. 2(a). The dimensions

of the mesa structure ($62 \times 400 \times 1.9 \, \mu m^3$) are measured by an atomic force microscope. A solid curve shown in Fig. 2(a) represents the I-V characteristic in the high-bias region above 1.0 V, while the upper right inset of Fig. 2(a) shows an overall I-V hysteresis loop typical of the outermost I-V branch of an IJJ system.[9] This I-V curve was obtained by the cyclic dc current scan. The finite voltage below $I = 13.8$ mA at $V \sim 0$ V, where all of the N_{max} IJJs are in the superconducting state, is caused by the contact resistance probably at the interface between Bi-2212 and Au films evaporated for electrodes.

During I-V measurements, we also monitored the output voltage from the bolometer as shown in Fig. 2(b). In this particular device, two radiation peaks (one at higher current with lower intensity and the other at lower current with higher intensity) were clearly observed. The maximum bolometer output of 13.7 mV at $V = 1.618$ V and $I = 11.5$ mA corresponds to approximately $0.2 \, \mu W$ according to the calibration of the sensitivity of the bolometer. Note that the total output power from the device should be evaluated separately by measuring the spatial radiation patterns,[11,12,16] since the solid angle of the detector window is only 3.2×10^{-3} sr. The radiation spectrum measured at 11.5 mA by the FT-IR spectrometer (JASCO Co., FARIS-1) is shown in the inset of Fig. 2(b), where a sharp emission peak at $f = 0.54$ THz is clearly observed. Using the ac Josephson relation with the contact resistance of 13 Ω, the number of resistive IJJs can be estimated to be $N = 1320$, which is in good agreement with $N_{max} \sim 1240$ given by the mesa height of 1.9 μm.

The actual imaging measurement has been performed with the following procedure: The pulse modulated THz wave was generated from the IJJ device by applying an additional square wave with a small amplitude (≤ 50 mV) at 10 kHz on the constant dc offset voltage using the function generator (Hewlett-Packard Co., 33120 A), because the HE bolometer has the best noise performance. The lock-in
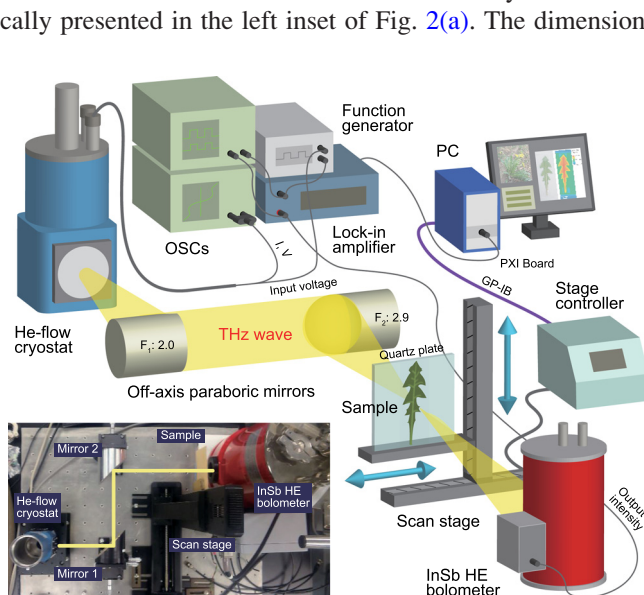

FIG. 1. Schematic diagram of the THz imaging system. The left lower photo presents the top view of the actual system.
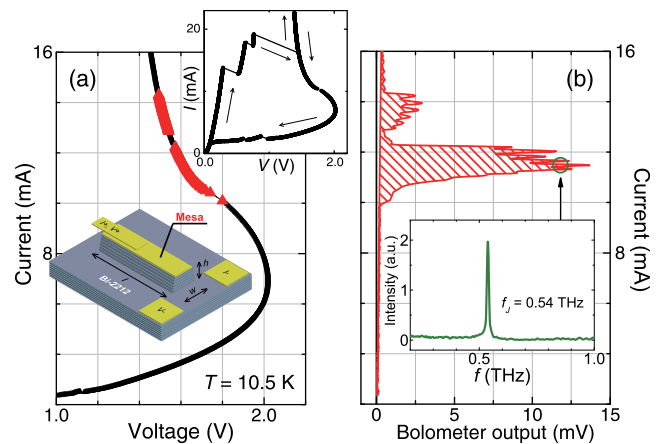

FIG. 2. (a) I–V characteristics of the IJJ oscillation device at bath temperature of $T = 10.5$ K. Red symbols on the curve indicate the specific I–V region where the intense THz wave emissions were observed as shown in (b). The upper right inset shows the overall I–V characteristic, when the current is driven as indicated by arrows. The left inset presents the schematic view of the IJJ device. (b) The current on the vertical axis common to Fig. 2(b) versus the bolometer output. The inset shows the radiation spectrum at 11.5 mA measured by the FT-IR spectrometer.

detection using such an electronic modulation is much better than the other methods such as the optical chopper one, since the far-infrared background noise due to the ambient spurious radiation can be avoided. The maximum intensity was then obtained by adjusting the offset level of the dc voltage and stabilized well to minimize the power fluctuations by adjusting the amplitude of the square wave. The imaging data are accumulated by simultaneous measurement of the sample positions (X, Z) and the bolometer output voltage. The output voltage is acquired by an AD converter installed in the PXI bus system (National Instruments Co.) through the analog output channel of the lock-in amplifier. Scanning parameters such as speed, step, and measurement area can be set by a homemade LabVIEW (National Instruments Co.) program. The obtained data are directly stored in the hard-disk drive and are simultaneously displayed on the PC screen in real time. The data set is stored in a ready-to-use spreadsheet file format for the convenience of the analysis.

III. RESULTS AND DISCUSSION

As test examples, THz images of two Japanese coins and a thin razor blade placed inside the brownish envelopes at $f = 0.537$ THz are shown in Figs. 3(a) and 3(b), respectively, while the actual photos of these objects are presented beside their THz images. In these measurements, the envelope was scanned in a horizontal direction at the speed of 32 mm/s. The screen size of Fig. 3(a) is 330×250 pixels corresponding to the measurement step of 0.2×0.2 mm^2, while those of Fig. 3(b) are 150×200 pixels and 0.4×0.4 mm^2, which were appropriately set in terms of the required spatial resolution. It took about 20 min to complete the data acquisition for Figs. 3(a) and 3(b), respectively. Note that the constancy of the bolometer output in the green area in Fig. 3(a), where there are no object absorbing incident THz waves, guarantees the time stability of the device. The signal-to-noise (S/N) ratio in these measurements exceeds 130, since the noise level is 0.1 mV in comparison to the maximum bolometer output of 13.7 mV (see Fig. 2(b)).

Here, all features of the transmission image associated with metallic and paper objects can be clearly seen. Especially, a hole of the 5-yen coin in Fig. 3(a) is very vividly seen, which has actually the diameter of 5 mm. The estimated spatial resolution of approximately 1 mm is compara-

ble with the expected Rayleigh limit. From Figs. 3(a) and 3(b), calculated transmittance of one sheet of paper is 79%, and it is clear that the metal is not transparent at all. It is interesting to note that the several interference fringe-like patterns in the deeper blue area in both Figs. 3(a) and 3(b) are clearly observed. Since the THz wave with the wavelength $\lambda = c_0/f = 0.558$ mm is multiply reflected at the inner walls of the envelope and interfered by itself, the interference condition can be expressed as $2d_m = (\lambda/2) \times 2m$, where d_m is the interspace distance of the inner walls and m is an integer. Hence, the distance between two neighboring fringes can be expressed as $d_{m+1} - d_m = \lambda/2 = 0.279$ mm. Since the thickness of the coin is 1.5 mm, at least $1.5/0.279 \sim 5-6$ fringes are expected to appear around the coins. This simple estimation agrees with the experimental result as shown in Fig. 3(a). Note that this interference effect is unique for the monochromatic THz waves, whose linewidth of about 0.5 GHz was separately obtained by a mixing technique.[14]

The beautiful interference fringe pattern encouraged us to construct a compact wavemeter to calibrate the wavelength of the monochromatic EM waves. The inset of Fig. 4 presents a schematic view of a wedge-shaped interferometer quartz cell composed of two flat quartz plates and stainless-steel insert. The raster scan technique was then used to a horizontal (X) direction, where interspace distance d linearly increases with X. Figure 4 shows the measured transmittance of the THz wave as a function of X which is oscillating approximately 20% in magnitude, where the negligible drift due to the focus shift is subtracted. From a least-square analysis with a sinusoidal wave, the frequency of the THz wave can be calculated to be $f_{cal} = 0.619$ THz ($\sigma = 0.0004$ THz, $R^2 = 0.958$), which is in good agreement with the value of 0.62 THz separately measured by a FT-TR spectrometer. In Fig. 4, an appropriate fitting curve is presented along with the experimental data.

The wedge-shaped quartz cell containing a liquid sample enables us to measure the absorption coefficient of polar liquids, e.g., water solutions. Figure 5 shows the
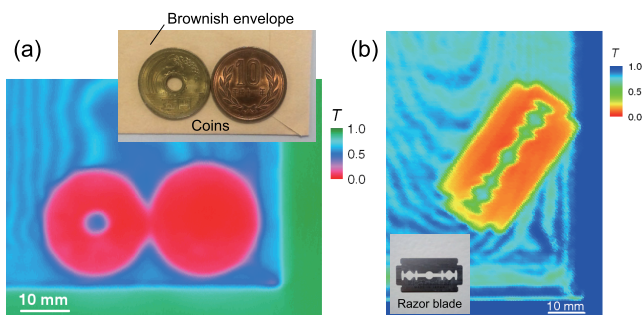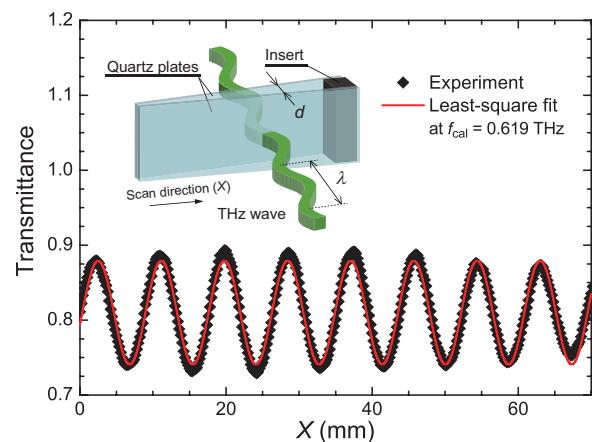
FIG. 3. THz images of 5-yen (left) and 10-yen (right) coins (a) and a razor blade (b) placed inside the brownish paper envelopes. The optical images of these objects are presented beside their THz images. In these images, transmittance T of the THz wave is plotted in each color-coded scale.

FIG. 4. Interference pattern which reflects the monochromatic THz wave. Black symbols represent the transmittance of the THz wave as a function of X, where X is proportional to interspace d as defined in the inset. The solid line shows a least-square fitting curve based on a sinusoidal wave at $f_{cal} = 0.619 \pm 0.0004$ THz.
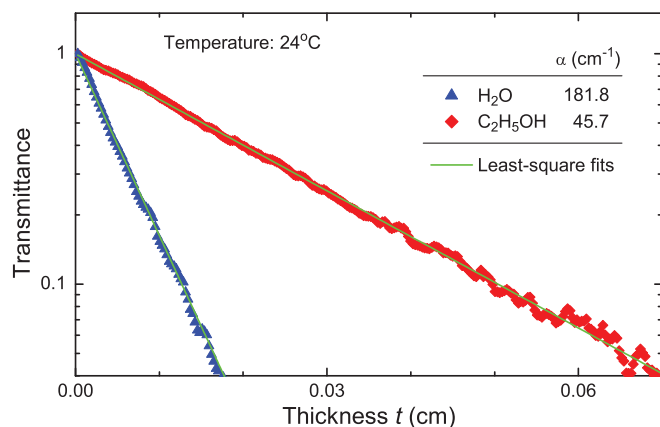
FIG. 5. Transmittance of the THz wave passing through distilled water (H_2O) and 99.5% pure ethanol (C_2H_5OH) as a function of sample thickness t at $f = 0.618$ THz. Two solid lines indicate the theoretical fitting expressed as $e^{-\alpha \cdot t}$. The inset shows the α-values obtained from the least-square fits.

transmittance of the THz wave at $f = 0.618$ THz passing through the distilled water (H_2O) and 99.5% pure ethanol (C_2H_5OH) at room temperature ($24\,^\circ$C) as a function of sample thickness t. Two solid lines in Fig. 5 are the best fit curves expressed as $e^{-\alpha \cdot t}$, where $\alpha = 181.8 \pm 1.5$ cm^{-1} for H_2O and 45.7 ± 0.1 cm^{-1} for C_2H_5OH are the obtained absorption coefficients. As demonstrated in Fig. 5, these α-values were obtained with great accuracy ($R^2 \simeq 0.996$). Especially for H_2O, the value is in good agreement with $\alpha \sim 180$, which has been previously obtained by the THz time-domain reflection spectroscopy[17,18] and transmission measurements.[19]

Although the large α-value above $100 \, \text{cm}^{-1}$ has made conventional transmission spectroscopy of liquid samples difficult due to the uncertainty of the sample thickness,[17–19] our simple method with a wedge-shaped quartz cell provides a useful technique for measuring the α-value very precisely. The noticeable advantages of using our technique are as follows: (1) Parameter-free measurement using simple absorption factor $e^{-\alpha \cdot t}$, where t can be accurately calibrated by the known radiation frequency; (2) high accuracy measurement with the large S/N ratio due to the high spectral intensity; (3) high frequency resolution, which is actually determined by the linewidth of the THz wave, typically ~ 0.5 GHz for the present IJJ device;[14] and (4) easy sample exchange, small amount of the liquid sample (≤ 0.01 cc), and short measurement time (e.g., 10 s for an α-value). By measuring the absorption spectra of liquid water in the THz region, where quantum effects are negligible ($kT = 208 \, \text{cm}^{-1}$), it is possible to investigate the intermolecular interactions due to permanent and induced dipole moments in the hydrogen bonded network of water molecules.[20] Our technique can also be applied to many other practical applications, such as substance identification, microanalysis of impurities, *in situ* observation of phase transitions, structure and dynamical analyses of large molecules, ions, and biological molecules in various solutions.

IV. SUMMARY

We have demonstrated the terahertz imaging by using high-T_c superconducting intrinsic Josephson junction oscillation devices, which emit the continuous and mono-chromatic terahertz electromagnetic wave around 0.6 THz with the spectral linewidth of 0.5 GHz. As test examples, terahertz images of Japanese coins and a razor blade placed inside the brownish paper envelopes were presented. Using a handmade interferometer quartz cell, we then investigated the interference patters to calibrate the radiation frequency. From a least-square analysis with a sinusoidal function, the radiation frequency was calculated with a relative accuracy of 0.1%. By injecting the distilled water and 99.5% pure ethanol into the quartz cell and measuring the sample thickness dependence of the transmittance of the THz wave, the absorption coefficients of these liquids were simply measured. The estimated errors of the obtained coefficients are $\leq 0.8\%$, which encourage us to make use of this technique for many other practical applications.

[1]M. Tonouchi, Nature Photon. **1**, 97 (2007).
[2]E. R. Brown, J. R. Söderström, C. D. Parker, L. J. Mahoney, K. M. Molvar, and T. C. McGill, Appl. Phys. Lett. **58**, 2291 (1991).
[3]H. Ito, F. Nakajima, T. Furuta, and T. Ishibashi, Semicond. Sci. Technol. **20**, S191 (2005).
[4]J. Faist, F. Capasso, D. L. Sivco, C. Sirtori, A. L. Hutchinson, and A. Y. Cho, Science **264**, 553 (1994).
[5]N. L. Rangel and J. M. Seminario, J. Phys. Chem. A **112**, 13699 (2008).
[6]O. V. Kibis, M. R. da Costa, and M. E. Portnoi, Nano Lett. **7**, 3414 (2007).
[7]K. Kawase, Opt. Photonics News **15**, 34 (2004).
[8]L. Ozyuzer, A. E. Koshelev, C. Kurter, N. Gopalsami, Q. Li, M. Tachiki, K. Kadowaki, T. Yamamoto, H. Minami, H. Yamaguchi, T. Tachiki, K. E. Gray, W.-K. Kwok, and U. Welp, Science **318**, 1291 (2007).
[9]R. Kleiner, F. Steinmeyer, G. Kunkel, and P. Müller, Phys. Rev. Lett. **68**, 2394 (1992).
[10]K. Kadowaki, H. Yamaguchi, K. Kawamata, T. Yamamoto, H. Minami, I. Kakeya, U. Welp, L. Ozyuzer, A. E. Koshelev, C. Kurter, K. E. Gray, and W. K. Kwok, Physica C **468**, 634 (2008).
[11]H. Minami, I. Kakeya, H. Yamaguchi, T. Yamamoto, and K. Kadowaki, Appl. Phys. Lett. **95**, 232511 (2009).
[12]M. Tsujimoto, K. Yamaki, K. Deguchi, T. Yamamoto, T. Kashiwagi, H. Minami, M. Tachiki, K. Kadowaki, and R. A. Klemm, Phys. Rev. Lett. **105**, 037005 (2010).
[13]B. D. Josephson, Phys. Lett. **1**, 251 (1962).
[14]T. Kashiwagi, M. Tsujimoto, T. Yamamoto, H. Minami, K. Yamaki, K. Delfanazari, K. Deguchi, N. Orita, T. Koike, R. Nakayama, T. Kitamura, M. Sawamura, S. Hagino, K. Ishida, K. Ivanovic, H. Asai, M. Tachiki, R. A. Klemm, and K. Kadowaki, Jpn. J. Appl. Phys., Part 1 **51**, 010113 (2012).
[15]H. Minami, M. Tsujimoto, T. Kashiwagi, T. Yamamoto, and K. Kadowaki, IEICE Trans. **E95-C**, 347 (2012).
[16]K. Kadowaki, M. Tsujimoto, K. Yamaki, T. Yamamoto, T. Kashiwagi, H. Minami, M. Tashiki, and R. A. Klemm, J. Phys. Soc. Jpn. **79**, 023703 (2010).
[17]C. Rønne, L. Thrane, P -O. Åstrand, A. Wallqvist, K. V. Mikkelsen, and S. R. Keiding, J. Chem. Phys. **107**, 5319 (1997).
[18]U. Møller, D. G. Cooke, K. Tanaka, and P. U. Jepsen, J. Opt. Soc. Am. B **26**, A113 (2009).
[19]J. T. Kindt and C. A. Schmuttenmaer, J. Phys. Chem. **100**, 10373 (1996).
[20]A. Luzar and D. Chandler, Nature **379**, 55 (1996).